Electronic Supplementary Material (ESI) for Journal of Materials Chemistry A.

The design of samples pressing

We have prepared tall cylinder samples for Bi_2Te_3-based polycrystalline materials to investigate the thermoelectric anisotropy [1]. However, for $Bi_2Te_{2.7}Se_{0.3}$ with nanoparticles its tall cylinder sample is easy to crack. In order to solve this problem we design a mould which can press a cuboid sample with size of 2 mm×10 mm×10 mm as shown in Fig. S1 (a) below. We measure thermal conductivity (κ) cut from the cuboid sample. The electrical conductivity is measured cut from the small cylinder with a diameter of 15 mm and thickness of 2 mm using another mould (in Fig. S1 (b) below). All these done is to assure the electrical conductivity and thermal conductivity measured along the same direction.

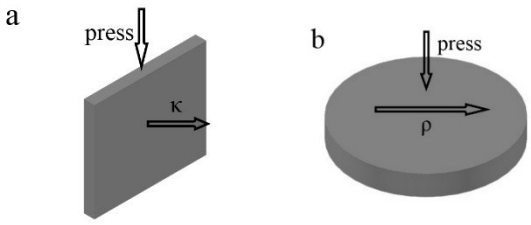

Fig. S1 Diagram of Samples pressed from two moulds

SEM Characterization of $Bi_2Te_{2.7}Se_{0.3}$ power grinded at different time and InSb power milled for 20 minutes

It can be seen that for $Bi_2Te_{2.7}Se_{0.3}$ power (Fig. S2 (a-e)) with increasing grinding time the grain size is smaller and more uniform. For InSb trank milled for 20 minutes, the material forms agglomerates with size of 100-

500nm (Fig. S2 (f)).

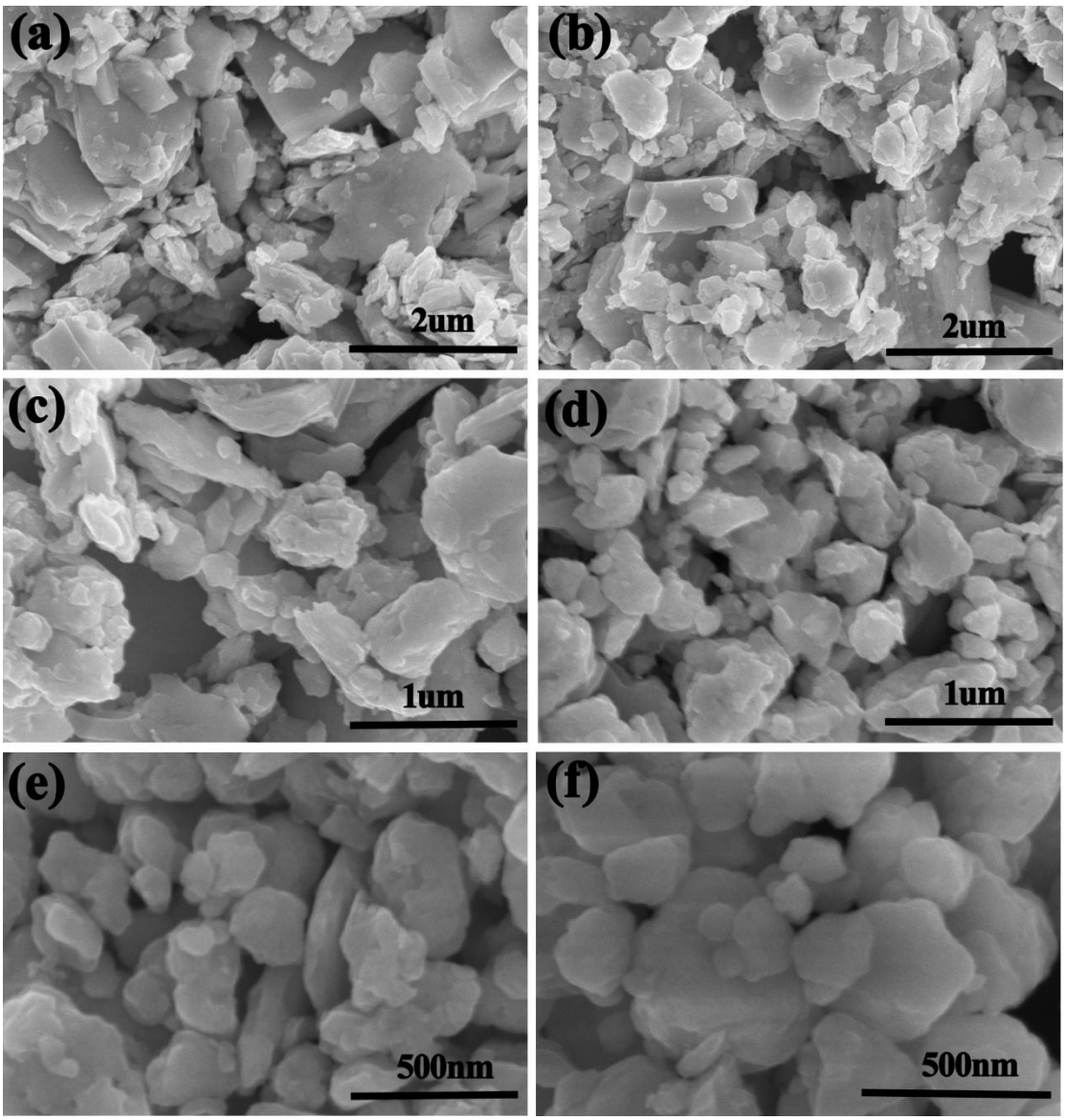

Fig. S2 FE-SEM micrographs of powders of $Bi_2Te_{2.7}Se_{0.3}$ grinded at different time (a) 0.5h, (b) 2.5h, (c) 4h, (d) 5.5h and (e) 7h; InSb (f) powder

TEM Characterization of $Bi_2Te_{2.7}Se_{0.3}$ power grinded at different time

The grain size of the grinded powders cannot be clearly recognized due to the aggregation. Seen from Fig. S3 (a-d) the particles are refined and uniform with increasing grinding time. The average particle size is 0.83μm, 0.54μm, 0.47μm and 0.36μm for $Bi_2Te_{2.7}Se_{0.3}$ grinded for 0.5h, 2.5h, 4h

and 5.5h, respectively.

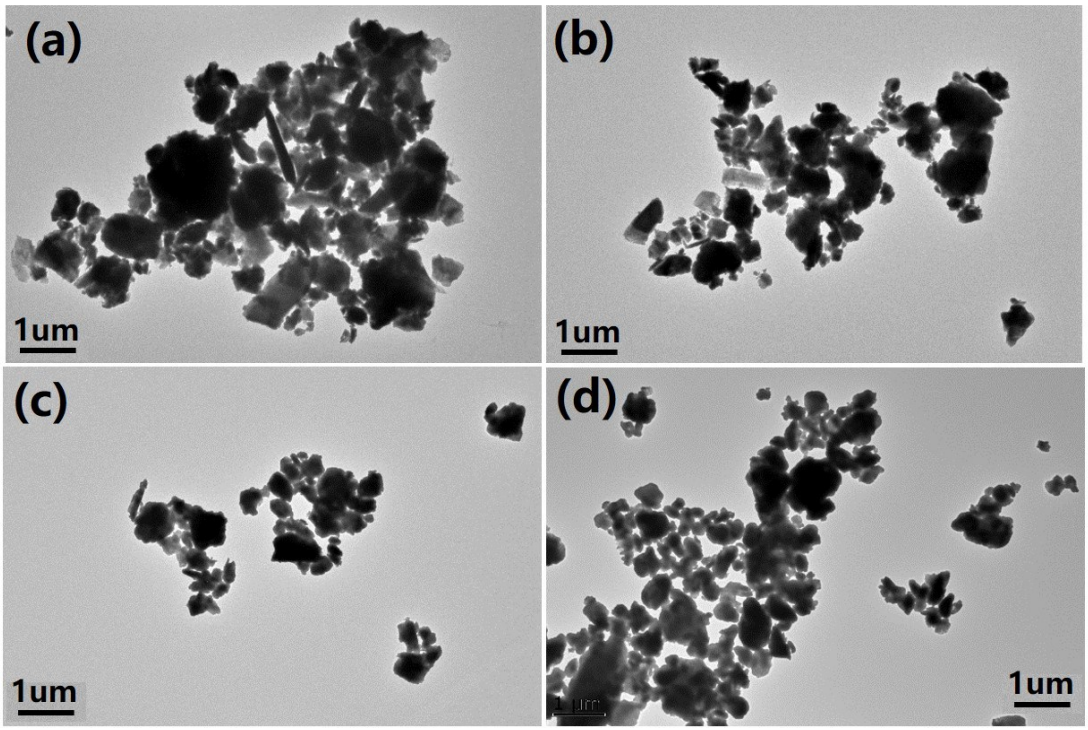

Fig. S3 TEM images for $Bi_2Te_{2.7}Se_{0.3}$ powder grinded for 0.5h (a), 2.5h (b), 4h (c) and 5.5h (d)

Microstructure Characterization of $Bi_2Te_{2.7}Se_{0.3}$ bulk sample and $Bi_2Te_{2.7}Se_{0.3}$-1.5%InSb bulk composite

Figure S4 shows the powder XRD patterns of $Bi_2Te_{2.7}Se_{0.3}$-*f*(InSb) (*f*=0, 1.0, 1.5, 2.0 and 2.5*vol%*) samples. The main diffraction peaks correspond well to the standard cards of $Bi_2Te_{2.7}Se_{0.3}$ (JCPDS No.50-0954), belonging to the hexagonal structure. Moreover, apart from the peaks of $Bi_2Te_{2.7}Se_{0.3}$, there is an additional small peak of 2θ=39.31° for the composite samples, which corresponds to the main peak of InSb (JCPS No.06-0208), indicating that there are two phases $Bi_2Te_{2.7}Se_{0.3}$ and InSb in the composite samples, no obvious other impurity phase being detected.

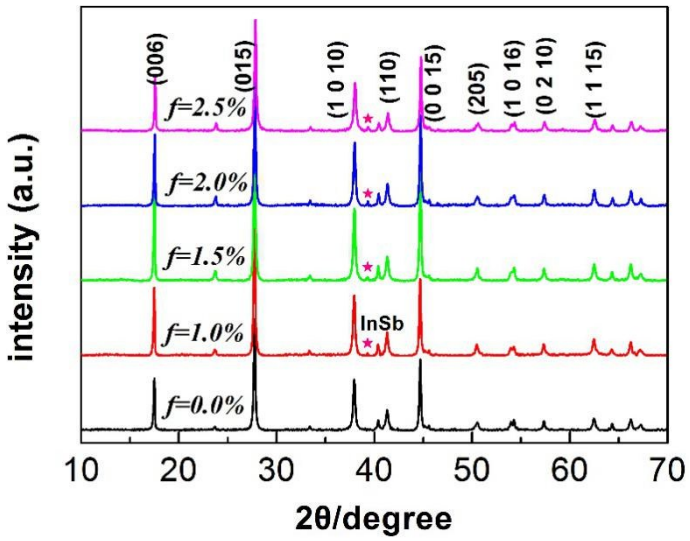

Fig. S4 powder XRD patterns of $Bi_2Te_{2.7}Se_{0.3}$-*f*(InSb) (*f*=0, 1.0, 1.5, 2.0 and 2.5*vol%*)

The bulk sample prepared from the powder suffered from long time grinding has smaller grain size. In addition, the highly oriented two-dimensional morphology of the bulk sample is presented for sample prepared from powder grinded for 0.5 hour (Fig. S5 (a)). With increasing grinding time the two-dimensional layered structure is weakened (Fig. S5 (e)). EDS seen Fig. S5 (g) using the selected rectangular area in Fig. S5 (f) confirms that InSb embedded in matrix of $Bi_2Te_{2.7}Se_{0.3}$.

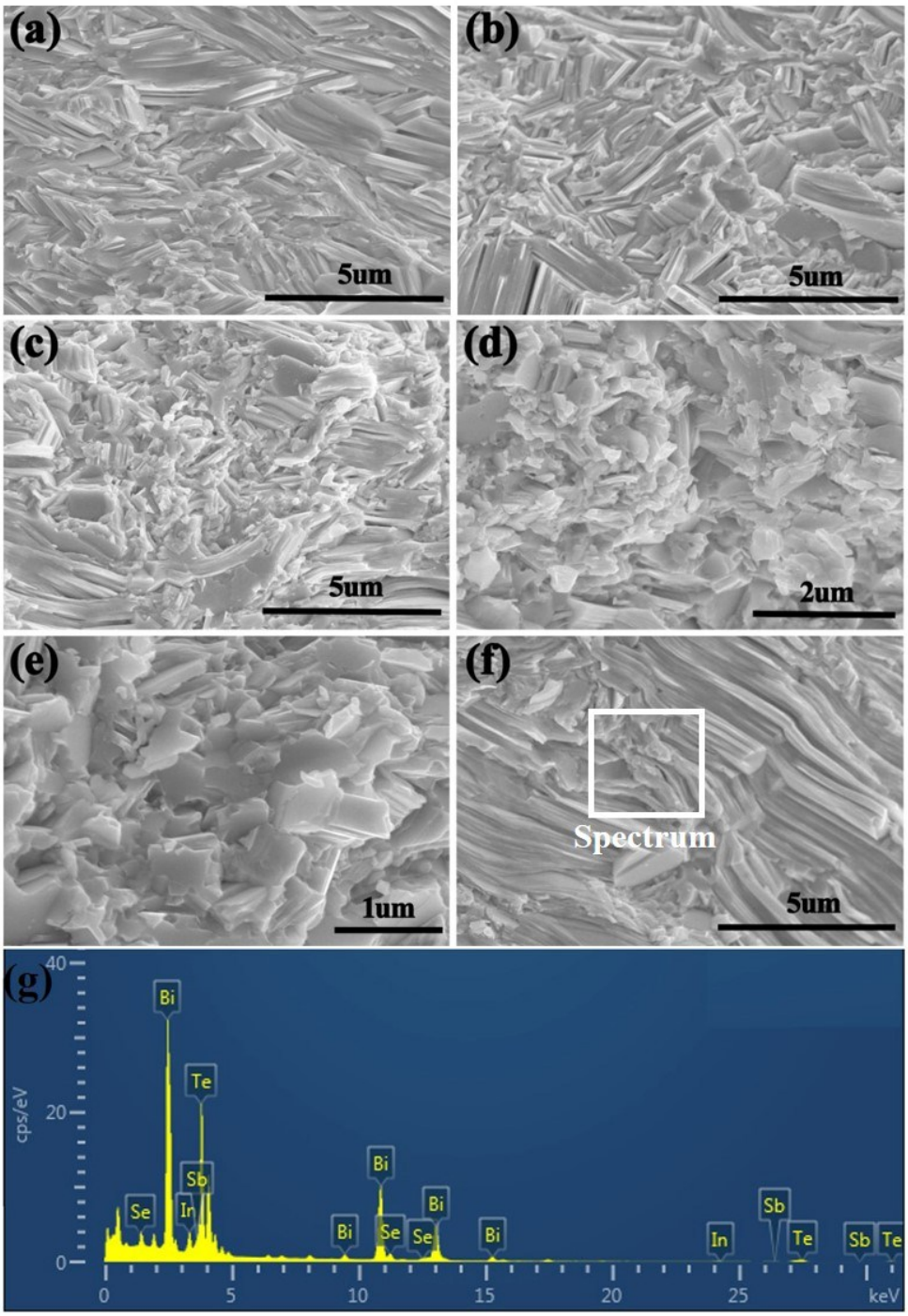

Fig. S5 (a) SEM images of the fracture surfaces of bulk materials compacted from $Bi_2Te_{2.7}Se_{0.3}$ powder grinded at different time (a) 1h; (b) 2.5h; (c) 4h; (d) 5.5h; (e) 7h; (f) the fracture surface of $Bi_2Te_{2.7}Se_{0.3}$-1.5%InSb bulk composite and (g) EDS of the selected rectangular area

Calculation of Lorenz numbers

According to the Wiedemann-Franz law, κ_C can be expressed as $\kappa_C = L\sigma T$,

where L is the Lorenz number. Employing the single parabolic band model, L can be determined by

$$L = (\frac{k_B}{e})^2[\frac{3F_2(\eta)}{F_0(\eta)} - \left(\frac{2F_1(\eta)}{F_0(\eta)}\right)^2]$$

with $$F_x = \int_0^\infty \frac{\varepsilon^x}{1 + exp(\varepsilon - \eta)} d\varepsilon$$

in which e is free electron charge, k_B is the Boltzmann constant, and η is the reduced Fermi level. The determination of η is based on the measured S, which is expressed as

$$S = \frac{k_B}{e}[\frac{2F_1(\eta)}{F_0(\eta)} - \eta]$$

based on the measured S, L can be determined, and their values are shown in figure S6(c) and figure S7(c).

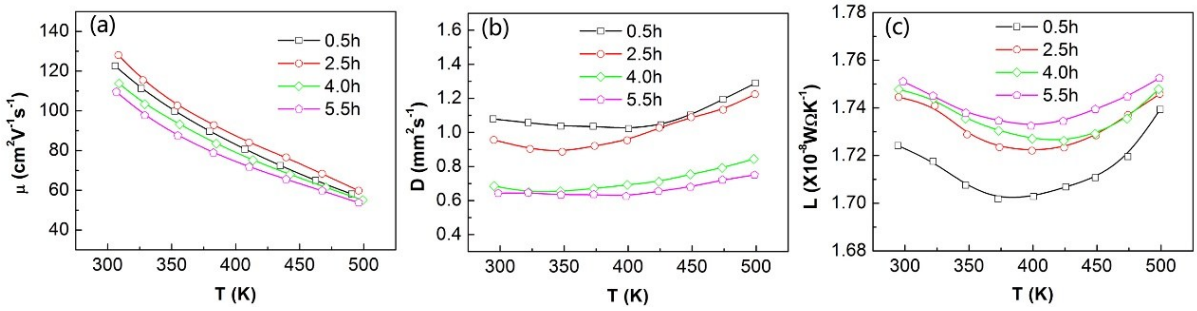

Fig. S6 Plot of mobility, thermal diffusion coefficient and Lorenz numbers[1] with temperature for $Bi_2Te_{2.7}Se_{0.3}$ grinded at different time

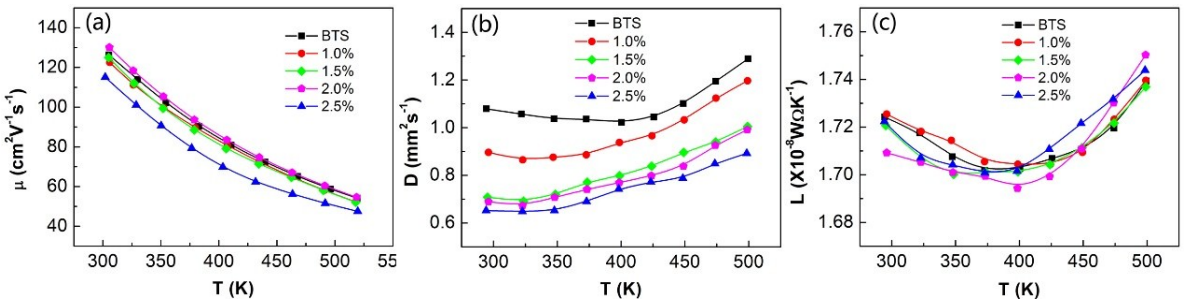

Fig. S7 Plot of mobility, thermal diffusion coefficient and Lorenz numbers with temperature for $Bi_2Te_{2.7}Se_{0.3}$-*f* InSb (*f*=0, 1.0, 1.5, 2.0 and 2.5*vol%*)

The results of the specifc heat, C_p, determined by DSC for $Bi_2Te_{2.7}Se_{0.3}$-*f*InSb (*f*=0, 1.0, 1.5, 2.0 and 2.5*vol%*) from 300 K to 523 K are shown in Fig. S8. The values of C_p range from 0.162 to 0.169 J g^{-1} K^{-1}, which are higher than the data reported by W. Liu[2], L. Hu[3] and W. S. Liu[4].

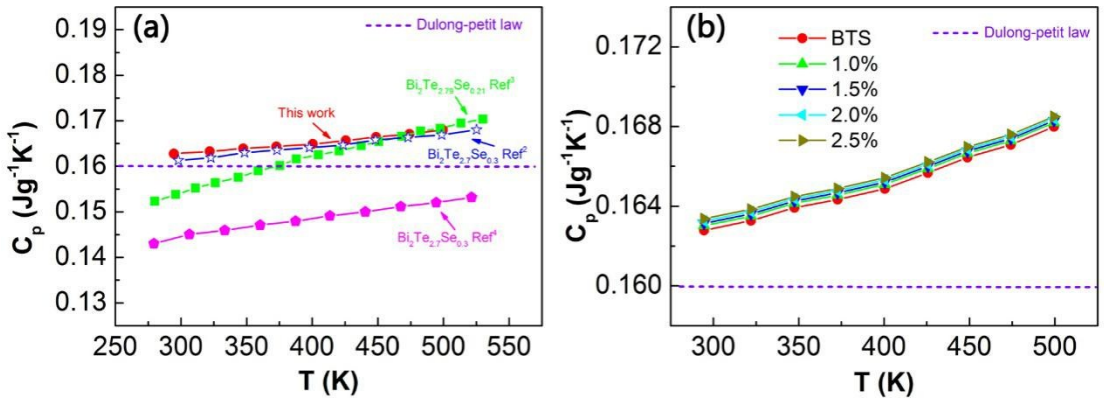

Fig. S8 Temperature dependences of the specific heat C_p determined by DSC for $Bi_2Te_{2.7}Se_{0.3}$-*f*InSb (*f*=0, 1.0, 1.5, 2.0 and 2.5*vol%*)

TEM image for $Bi_2Te_{2.7}Se_{0.3}$-1.5%InSb grains

Figure S9 (a) is a low magnification TEM image of $Bi_2Te_{2.7}Se_{0.3}$-1.5%InSb grains. It can be seen that many small dark dots with size of 5-100nm are embedded in gray matrix. Figure S9 (b) presents the EDS element from the dark pot of Fig. S9 (a) showing InSb. Those nanophases are also visible in the X-ray diffraction (XRD) spectra (figure S4). Figure S9 (c) shows the EDS element of the matrix, which confirms it is $Bi_2Te_{2.7}Se_{0.3}$. Detailed

quantitative analysis indicates that elemental ratios of Bi, Te, and Se are close to the nominal compositions.

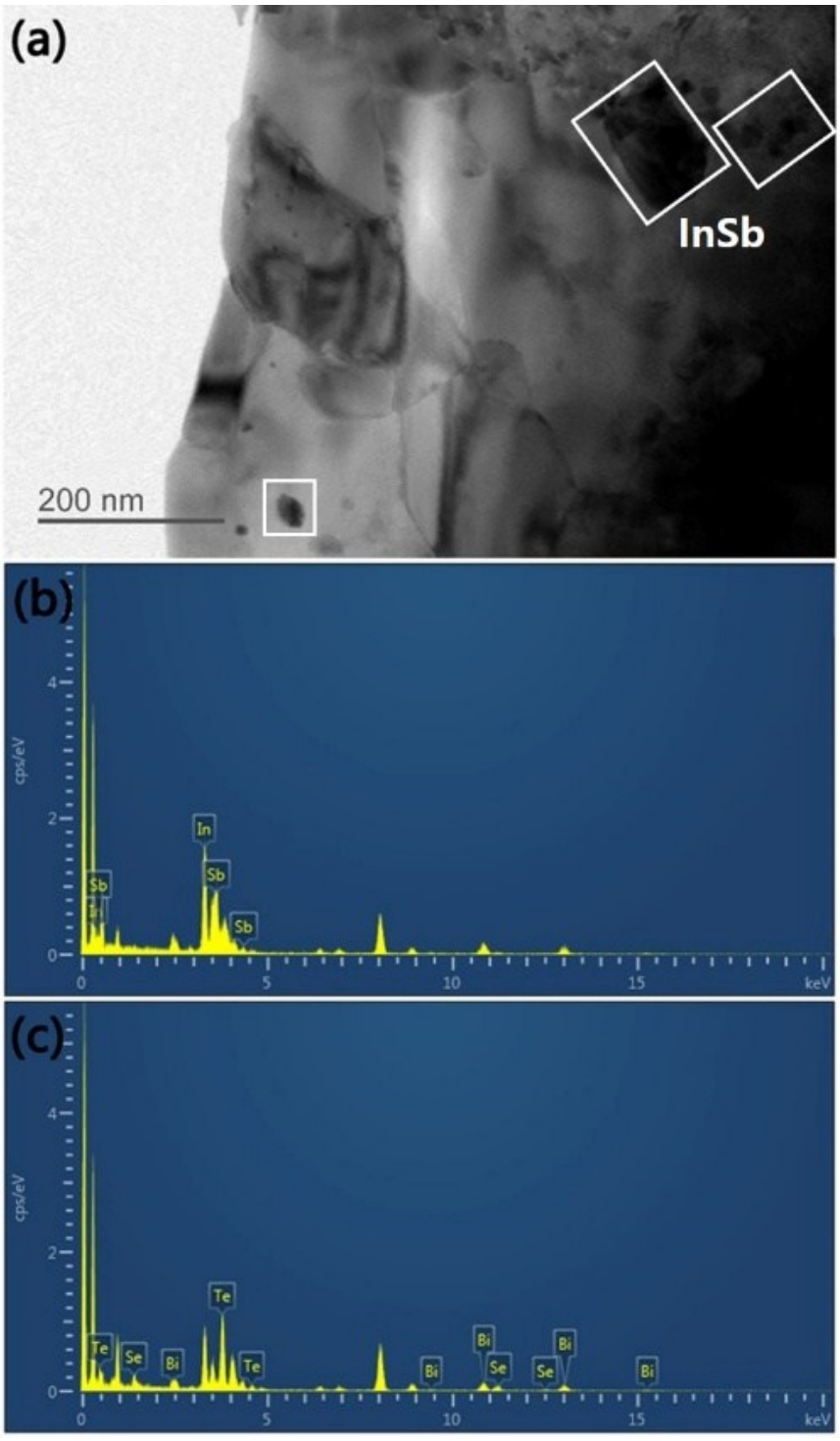

Fig. S9 (a) TEM image of $Bi_2Te_{2.7}Se_{0.3}$-1.5%InSb, (b) EDS for InSb and (c) EDS for matrix

Repeatability of thermoelectric properties for $Bi_2Te_{2.7}Se_{0.3}$-1.5%InSb

To confirm the reproducibility of results, three samples are measured as shown in Fig. S10. Sample 1 and sample 2 are the two sample of the same batch. Sample 2 and sample 3 are the two sample of different batch with same composition. The experimental results indicate that our samples have good reproducibility.

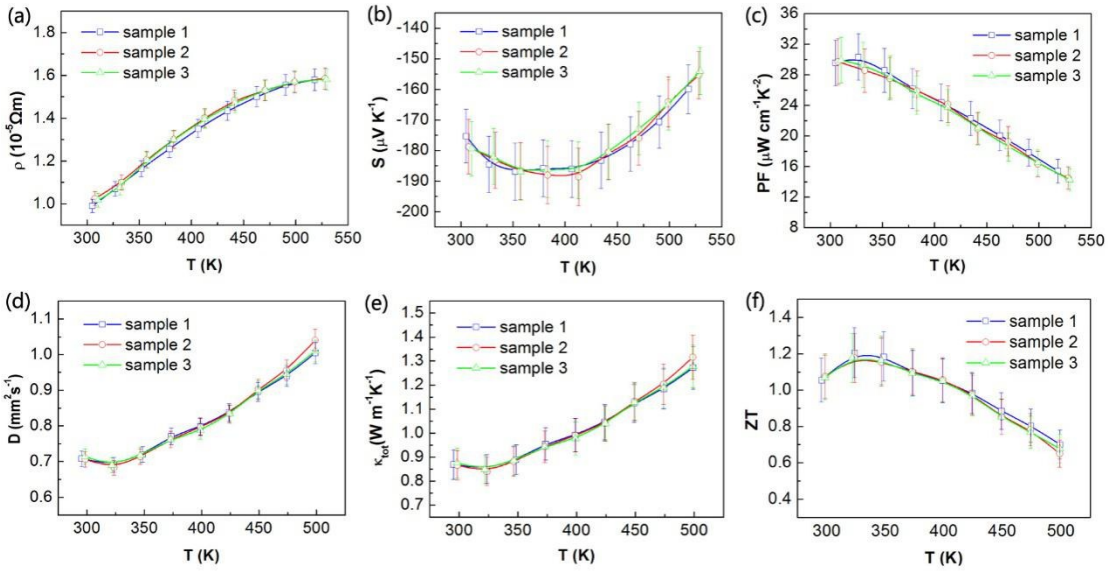

Fig. S10 Repeatability of thermoelectric properties for $Bi_2Te_{2.7}Se_{0.3}$-1.5%InSb

Calculation of Lattice Thermal Conductivity

To estimate the effects of the different phonon scattering processes, the lattice thermal conductivity was theoretically analyzed using Debye-Callaway model [5]

$$\kappa_L = \frac{k_B}{2\pi^2 v}\left(\frac{k_B T}{\hbar}\right)^3 \int_0^{\frac{\Theta_D}{T}} \tau_{tot} \frac{z^4 exp(z)}{[\exp(z)-1]^2} dz$$

where $x=\hbar\omega/k_BT$ is the reduced phonon energy, ħ is the reduced Planck constant, k_B is the Boltzmann constant, ω is the phonon frequency, θ_D is the Debye temperature, v_s is the average speed of sound calculated from $v=(v_l^{-3}/3+2v_t^{-3}/3)^{-1/3}$, τ_{tot} is the combined relaxation time for phonon scattering processes. And τ_{tot} can be calculated as the sum of the reciprocal relaxation time of all the different scattering process: $\tau_{tot}^{-1}(\varpi) = \Sigma_i\tau_i^{-1}(\varpi)$ [6]. The phonon scattering pathways generally include phonon-phonon Umklapp (U), electron-phonon (E), point defects (PD), and grain boundaries (B). The relevant phonon relaxation times are given by

Umklapp phonon scattering

$$\tau_u^{-1} = \frac{\hbar\gamma^2\omega^2T}{\overline{M}v^2\Theta_D}exp(-\frac{\Theta_D}{3T})$$

Electron phonon scattering

$$\tau_E^{-1} = \frac{E_{def}^2 m^* \omega^2}{2\pi\hbar^3\rho v}$$

Point defect phonon scattering

$$\tau_{PD}^{-1} = \frac{\overline{V}\omega^4}{4\pi v^3}\Gamma$$

and dislocation strain phonon scattering

$$\tau_{DS}^{-1} = 0.6B_D^2N_D(\gamma+\Delta\gamma)^2\omega\{\frac{1}{2}+\frac{1}{24}\left(\frac{1-2r}{1-r}\right)^2[1+\sqrt{2}(\frac{v}{v_\perp})]^2\}$$

where N_D is the dislocation density, B_D is the effective Burger's vector, r is the Poisson's ratio and) Δγ is the change in γ due to the dislocation strain, as given by

$$\Delta\gamma = \frac{V_{BT} c_0 K}{k_B T_a}(\gamma\alpha^2 - \alpha\beta)$$

With $$\alpha = \frac{V_{BS} - V_{BT}}{V_{BT}}$$

$$\beta = \frac{M_{BT} - V_{BT}}{2M_{BT}}$$

where c_0 is the concentration of InSb in $Bi_2Te_{2.7}Se_{0.3}$, K is the bulk modulus of $Bi_2Te_{2.7}Se_{0.3}$, T_a is the sample sintering temperature, V_{BS} and V_{BT} are the atomic volume of Bi_2Se_3 and Bi_2Te_3, and M_{BS} and M_{BT} are the atomic mass of Bi_2Se_3 and Bi_2Te_3.

According to the Matthiessen rule 6 the total scattering relaxation time τ_{tot} can be given by U+E+PD+B mode

$$\tau_{tot}^{-1} = \tau_U^{-1} + \tau_E^{-1} + \tau_{PD}^{-1} + \tau_B^{-1}$$

U+E+PD+B+D model

$$\tau_{tot}^{-1} = \tau_U^{-1} + \tau_E^{-1} + \tau_{PD}^{-1} + \tau_B^{-1} + \tau_{DC}^{-1} + \tau_{DS}^{-1}$$

By inputting physical parameters listed in Table I into above equations, κ_L can be calculated by models of U+E+PD+B and U+E+PD+B+D.

Table I Physical properties for $Bi_2Te_{2.7}Se_{0.3}$ used to calculate κ_L based on various phonon scattering processes.

Parameters	Values
Debye temperature Θ_D	164 [7]
Longitudinal sound velocity υ_L (ms^{-1})	2800 [7]

Transverse sound velocity υ_T (ms^{-1})	1600 [7]
sound velocity υ (ms^{-1})	1778
Average atomic mass of $Bi_2Te_{2.7}Se_{0.3}$ (kg)	2.612×10^{-25}
Average atomic volume of $Bi_2Te_{2.7}Se_{0.3}$ (m^3)	3.45×10^{-29}
Sample density ρ of $Bi_2Te_{2.7}Se_{0.3}$ (g cm^{-3})	7.1
Grain size for $Bi_2Te_{2.7}Se_{0.3}$ (nm)	830
Point defect scattering parameter Γ	0.18
Dislocation density N_D of $Bi_2Te_{2.7}Se_{0.3}$ (cm^{-2})	1.7×10^{11}
Magnititude of Burger's vector B_D of $Bi_2Te_{2.7}Se_{0.3}$ (Å)	27
Poisson's ratio *r*	0.4 [8]
Gruneisen parameter	1.5 [9]
Bulk modulus (GPa)	37.4 [7]

For BTS-InSb composite the additional parameters ΔD ($2.04 gcm^{-3}$), R (30nm) and V_P ($3\times10^{15}cm^{-3}$) should be added besides the parameters listed in Table I to calculate the phonon scattering of precipitates.

Reference

1. D. Li, X. Y. Qin, J. Zhang, C. J. Song, Y. F. Liu, L. Wang, H. X. Xin and Z. M. Wang, RSC Adv., **2015**, 5, 43717.

2. W. Liu, K. C. Lukas, K. McEnaney, S. Lee, Q. Zhang, C. P. Opeil, G. Chen, Z. F. Ren, *Energy & Environmental Science* 2013, 6, (2), 552.

3. L. P. Hu, H. J. Wu, T. J. Zhu, C. G. Fu, J. Q. He, P. J. Ying, X. B. Zhao, Adv. Energy Mater., 2015, 5, 1500411.

4. W. S. Liu, Q. Y. Zhang, S. Cheng, Y. C. Lan, S. Chen, X. Yan, Q. Zhang, H. Wang, D. Z. Wang, G. Chen, Z. F. Ren, Adv. Energy Mater. 2011, 1, 577.

5. C. Fu, S. Bai, Y. Liu, Y. Tang, L. Chen, X. Zhao, T. Zhu, Realizing high figure of merit in heavy-band p-type half-Heusler thermoelectric materials, Nat. Commun. 2015, 6, 8144.

6. N.W. Ashcroft, N.D. Mermin, Solid State Physics, Brook/Cole/Thomson Learning,New York, 1976.

7. J. Jenkins, J. Rayne, R. Ure, Phys. Rev. B 1972, 5, 3171-3184.

8. T. Clin, S. Turenne, D. Vasilevskiy, R. A. Masut, J. Electron. Mater. 2009, 38, 994.

9. X. Chen, H. D. Zhou, A. Kiswandhi, I. Miotkowski, Y. P. Chen, P. A.

Sharma, A. L. Lima Sharma, M.A. Hekmaty, D. Smirnov, Z. Jiang, Appl. Phys. Lett. 2011, 99, 261912.